Springer

KSME

Journal of Mechanical Science and Technology 24 (2) (2010) 537~543
www.springerlink.com/content/1738-494x
DOI 10.1007/s12206-010-0103-3

The effect of channel flow pattern on internal properties distribution of a proton exchange membrane fuel cell for cathode starvation conditions †

Dong-Soo Ko[1], Young-Min Kang[1], Jang-Sik Yang[2], Ji-Hwan Jeong[3], Gyung-Min Choi[3,*] and Duck-Jool Kim[2]

[1]*Graduate School of Mechanical Engineering, Pusan National University, Busan, 609-735, Korea*
[2]*RIMT, Pusan National University, Busan, 609-735, Korea*
[3]*School of Mechanical Engineering, Pusan National University, Busan, 609-735, Korea*

(Manuscript Received February 11, 2009; Revised September 14, 2009; Accepted October 21, 2009)

Abstract

The effect of channel flow pattern on the internal properties distribution of a proton exchange membrane fuel cell (PEMFC) for cathode starvation conditions in a unit cell was investigated through numerical studies and experiments. The polarization curves of a lab-scale mixed serpentine PEMFC were measured with increasing current loads for different cell temperatures (40, 50, and 60°C) at a relative humidity of 100%. To study the local temperature on the membrane, the water content in the MEA, and the gas velocity in terms of the channel type of the PEMFC with operating characteristics, numerical studies using the es-pemfc module of STAR-CD, which have been matched to the experimental data, were conducted in detail. The water content and velocity at the cathode channel bend of the mixed serpentine channel were relatively higher than those at the single and double channels. Conversely, the local temperature and mean temperature on the membrane of a single serpentine channel were the highest among all channels. These results can be used to design the PEMFC system, the channel flow field, and the cooling device.

Keywords: PEMFC; Internal properties; Channel flow; And starvation condition

1. Introduction

A proton exchange membrane fuel cell (PEMFC) has many advantages such as high energy density, operability at room temperature, quick start-up, quick response to load, and environment-friendly high efficiency [1, 2]. The performance of the PEMFC can be improved by optimizing its operating parameters, such as gas flow rate, operating cell temperature, inlet pressure, humidity condition, and channel flow type. However, the optimization of these parameters for the PEMFC depends on each operating condition [3-9].

Flooding due to poor water management may sometimes block the channel, the porous gas diffusion layer, and the catalyst layer. Poor thermal management at the startup of the fuel cell may cause the internal temperature in the fuel cell to drop to below zero, which can freeze the condensed water and can in turn result in the starvation of feed due to the blocked porous layers in the gas diffuser layer [10-13]. In the anode starvation condition, the performance of the fuel cell will degrade and the cell voltage would drop. The cell potential will reverse, giving rise to a negative potential difference between the anode and the cathode. Cell reversal will accelerate the corrosion of the carbon components, leading to a serious explosion if oxygen mixes with hydrogen [14-15].

It is difficult to maintain a constant current with load changes, especially in the cathode starvation. A current overshoot results in the degradation of the cell performance [16-

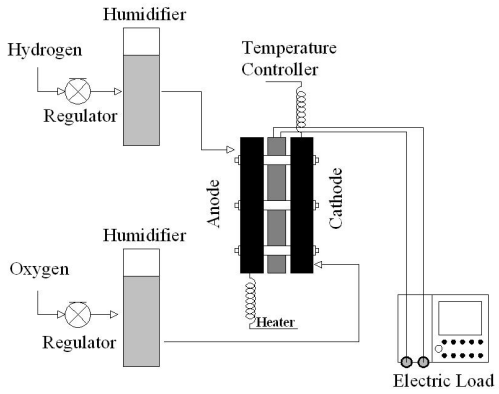

Fig. 1. Schematic diagram of the experimental setup.

† This paper was recommended for publication in revised form by Associate Editor Tong Seop Kim

*Corresponding author. Tel.: +82 51 510 2476, Fax.: +82 51 510 5236
E-mail address: choigm@pusan.ac.kr

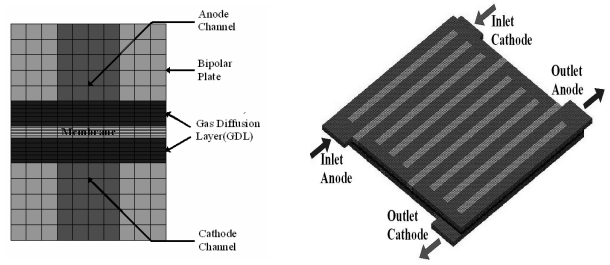

Fig. 2. Channel grid arrangement (a) and counterflow mixed serpentine channel (b).

18]. Studies on the starvation conditions of the PEMFC, however, are still insufficient.

Liu et al. [19] measured the polarization curves of a segmented single fuel cell under starvation conditions. However, the concentration distributions in the MEA for the cathode starvation condition were not understood in detail.

Water and heat management is an important factor in the uniform distribution of current density and water contents on the membrane for different channel flow patterns [20-23]. Many researchers have investigated the internal characteristics information of the PEMFC through numerical studies.

Kazim et al. [24] studied the current density and internal distribution of the PEMFC with interdigitated flow by a two-dimensional numerical study. However, this study was conducted using a simple model application and only one channel flow.

Wang et al. [25, 26] studied the internal current density in the MEA and the performance change of the PEMFC with interdigitated and parallel flow by a three-dimensional numerical study. Simpalee et al. [27, 28] studied the internal distribution on the rib parts and channel one areas in the gas diffusion layer (GDL). However, the effect of channel pattern on the internal distributions of a PEMFC was not studied.

In this study, the effect of channel flow pattern on the distribution of internal properties in a counterflow PEMFC for the cathode starvation conditions was investigated in detail through numerical studies and experiments.

2. Experimental distributions and numerical model

2.1 Experimental apparatus

Fig. 1 shows the schematic diagram of a lab-scale experimental setup of a PEMFC. Generally, hydrogen is supplied to the anode and air to the cathode to operate fuel cells.

However, in this study, oxygen - instead of air - was supplied to the cathode under a limited surrounding environment to observe the electrochemical reaction between hydrogen and oxygen. The stoichiometry ratio of hydrogen was fixed to 1.2, while oxygen supplied was 0.6 for cathode starvation to match with the experiment conditions. Reactant gases were supplied at a relative humidity of 100% by humidifiers and were transported in the fuel cell system through unipolar plates. The

Table 1. Grid geometry dimension and properties.

Channel	
Inlet area[mm^2]	0.6
Active area[mm^2]	23.04
GDL	
Thickness [mm]	0.25
Permeability [m^2]	1.0E-12
Porosity [%]	0.7
Thermal conductivity [W/mK]	0.25
MEA	
Membrane thickness [mm]	0.05
Thermal conductivity [W/mK]	0.15
Dry membrane density [g/cm^3]	2
Equivalent weight of dry membrane[g/cm^3]	1100
Cathode exchange current density [A/cm^2]	20
Cathode transfer coefficient	0.6
Anode exchange current density [A/cm^2]	200
Anode transfer coefficient	1.2

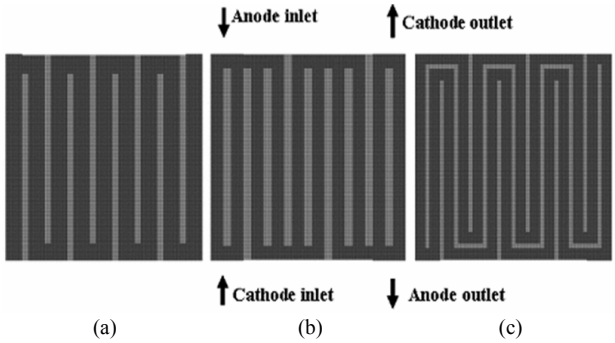

Fig. 3. Channel flows of single (a), double (b), and mixed serpentine (c).

operating cell temperatures of the end plates were controlled by cartridge heaters and temperature sensors. The end plates were maintained at cell temperatures of 40, 50, and 60°C. Experimental data were obtained by the application of an electric load of KIKUSUI PLZ-164WA.

2.2 Numerical apparatus

A control volume technique based on a commercial flow solver, STAR-CD, was used to solve the governing equations. This software is used with an add-on tool called Expert System for PEMFCs, which provides the source terms for species transport equations, phase change equations for water, and heat generation equations.

Fig. 2 shows the mixed serpentine channel of counter flow, which is modeled in the channel numerical calculation and in the channel grid arrangement. The active area of the fuel cell was 4.8×4.8 cm^2. Table 1 shows the grid geometry dimensions and properties. The grid arrangement diagram was divided into five sub-regions: anode gas channel and bipolar

plate, gas diffusion layer, membrane, gas diffusion layer, cathode gas channel, and bipolar plate. The effect of cell temperature on cell performance is quite complex, as the cell voltage depends on the catalyst activation of the cathode side, CO poisoning of the anode side, humidity in the membrane, and gas diffusivity in the gas diffusion layer. As the water starts to boil at about 60°C, the cell temperature conditions were selected to investigate the effect of evaporation on cell performance.

Fig. 3 shows the counterflow channel of single, double, and mixed serpentine. The gas flow was assumed to be steady-state, laminar, and incompressible.

Table 2 shows the operation conditions, while Table 3 shows the equations used in the calculation.

3. Results and discussion

3.1 Internal distributions of mass characteristics for various channel flows

Fig. 4 shows the polarization curves for three different cell temperatures, 40, 50, and 60°C, at the relative humidity of 100%.

These curves were used to compare the experimental results with the numerical ones for the standard and cathode starvation conditions. The numerical results showed good agreement with the experimental ones.

The contact resistance decreased with the increasing cell temperature at a full humidity condition. The performance of the PEMFC was improved with the increase in temperature for the standard condition. However, in the case of the cathode starvation condition, the highest performance was obtained at a cell temperature of 50°C.

The performance of the fuel cell at 60°C might drop significantly due to the drying of the membrane for the cathode starvation condition. In the present experiment, the flow rates of O_2 and H_2 were set to 20 cc/min and 50 cc/min, respectively. However, for the standard condition, 80 cc/min of H_2 and O_2 was supplied. This large mass flow rate might result in a slight difference between CT 50 and CT 60.

Fig. 5 shows the results of the local temperature on the membrane, water content in the MEA, and velocity of gas in the channel with changing channel flows (single, mixed, and double channel) at a cell temperature of 50°C and 85.5 mA/cm^2 for both standard and cathode starvation conditions. The upper and bottom parts show the result of the standard condition and the cathode starvation condition, respectively.

The temperature in the periphery of the gas inlet regions was higher than that of the other regions for both standard and cathode starvation conditions. Especially the temperature at the cathode inlet region, the starvation condition increased extremely up to the local maximum temperature of about 65°C. The difference in the local maximum temperature be-

Table 2. Operation condition.

Stoichiometry ratio [H_2, O_2]	1.2, 0.6
Flow rate [H_2, O_2(cc/m)]	50, 20
Cell temperature [℃]	40, 50, 60
Inlet humidity condition [%]	100
Operating pressure [atm]	1

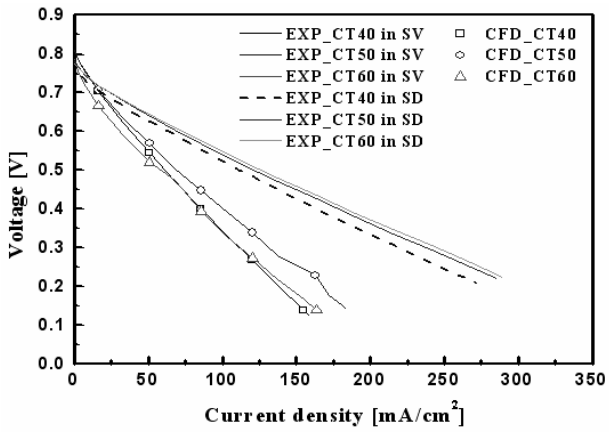

Fig. 4. I-V polarization curves obtained by experiments and numerical simulations for three cell temperatures at relative humidity of 100%.

Table 3. Equations used for the calculations.

	Express	Ref. No
Butler-Volmer equation	$I = i_o\{\exp[\frac{-\alpha_{Rd}F(E-E_r)}{RT}] - \exp[\frac{\alpha_{OX}F(E-E_r)}{RT}]\}$	2
Current density	$I(x,y) = \frac{\sigma_m}{t_m}\{E - V_{cell} - \eta(x,y)\}$	29
Conductivity	$\sigma_m = (\left(0.514\frac{M_{m,dry}}{\rho_{m,dry}}C_{wk} - 0..26\right)e\left(1268\left(\frac{1}{303}-\frac{1}{T}\right)\right) \qquad \lambda = \frac{M_{m,dry}}{\rho_{m,dry}}C_{wk}$	30
Water content	$\lambda_a = \lambda_c = \begin{cases} 0.043+17.81a-39.85a^2+36.0a^3 \; for & 0<a\le 1 \\ 14.0+1.4(a-1) \; for & 1<a\le 3 \end{cases} \qquad a_k = \frac{X_{w,K}P(x,y)}{P^{sat}{}_{w,K}}$	31
Heat energy	$\Delta H_T = \Delta H_{298.15} + \Delta a(T-298.15) + \Delta b\frac{(T-298.15)^2}{2} - \Delta c\frac{(T-298.15)^3}{3}$ $\Delta S_T = \Delta S_{298.15} + \Delta a\ln\left(\frac{T}{298.15}\right) + \Delta b(T-298.15) - \Delta c\frac{(T-298.15)^2}{2}$	2

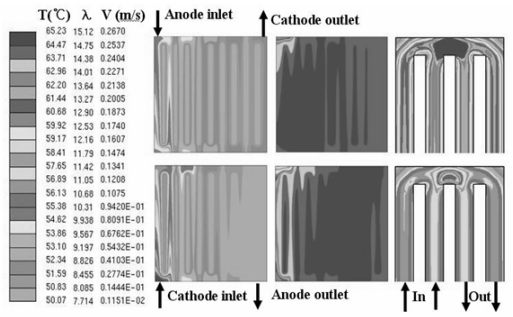

(a) Single channel flow

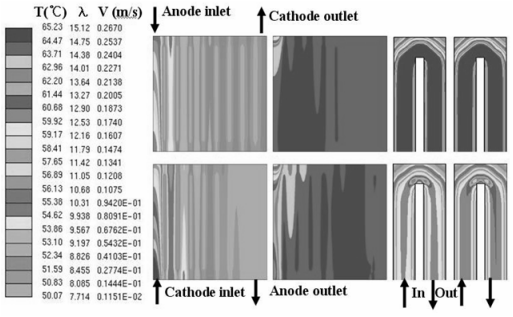

(b) Mixed channel flow

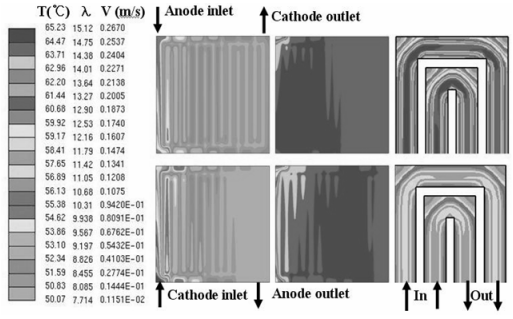

(c) Double channel flow

Fig. 5. Distributions of local temperature, water content in the MEA, and velocity at 85.5 mA/cm^2 with a cell temperature of 50°C (upper, standard condition, bottom, starvation condition).

tween the standard and the starvation condition exceeded 5°C, but the temperature distribution became almost uniform at the outlet region.

The local maximum temperature was in the order of single > double > mixed channel. Particularly, the local temperature in the single channel for the starvation condition increased up to 67°C, and the temperature gradient of the channel bend became higher than those of other channels.

For the water content distribution in the MEA, drying out was observed at the inlet region on the anode for all conditions, especially for the starvation condition. Water content of the rib parts was higher than that of the channel parts.

In terms of the water content distribution in the MEA for the starvation condition, water content at the outlet region was higher than that at the inlet region. This low concentration at the inlet region is caused by the drying out in the cathode inlet region for the starvation condition, unlike in the standard condition.

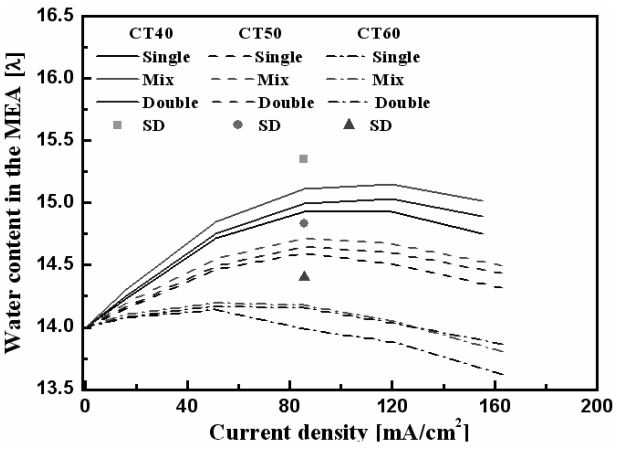

Fig. 6. Water content for various channel flows for the cathode starvation (lines) and standard condition (symbols).

The drying out was due to the poor water production caused by the insufficient feeding of oxygen in the initial condition and the evaporation of the produced water through the reaction heat and surrounding temperature. In addition, cathode starvation enhanced the locally concentrated reaction at the inlet region, which resulted in a large temperature gradient on the membrane.

The water content in the MEA was the in the order of mixed > double > single channel. The distribution of the water content in the MEA was relatively uniform in the mixed serpentine channel.

The gas velocities in the cathode starvation condition were almost the same, regardless of the flow pattern. The velocity in the channel bend was relatively high. Channel velocity decelerated to half of that for the starvation condition due to the shortage of oxygen at the cathode. The current density distribution reflected the velocity of oxygen on the membrane, which is caused by poor exhaust at the channel bend for the starvation condition.

The mean velocity of gas in the cathode channel was in the order of single > double > mixed channel. Conversely, the velocity at the mixed channel bend was the fastest among those at the other channels. As two straight channels combined to form one channel at the channel bend part, the mixed serpentine flow had high momentum, which was useful for exhausting the condensed water in the channel bend and might also be useful for water management.

3.2 Water content for various channel flows

Fig. 6 shows the water content in the MEA as a function of the current density and cell temperatures. After reaching its peak values, the water content tended to decrease with the increasing current density.

The current density at the maximum water content of each condition moved to a lower value along with increasing cell temperature for the cathode starvation condition.

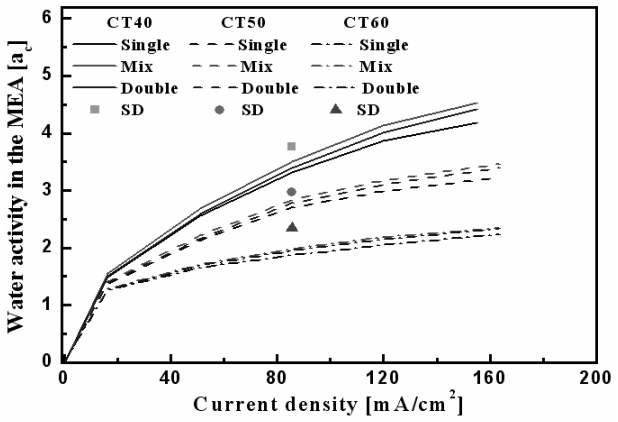

Fig. 7. Water activity at the cathode for various channel flows.

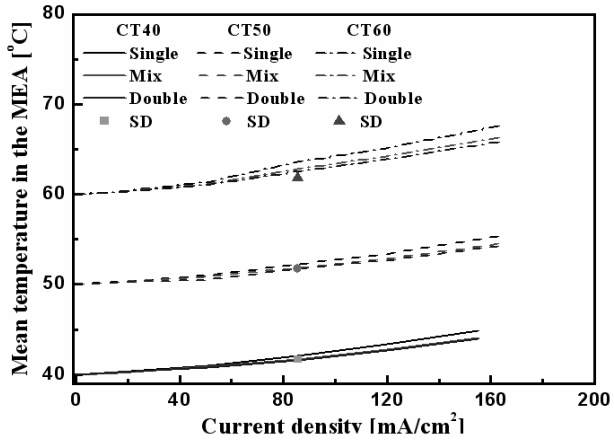

Fig. 8. Mean temperature for the various channel flows.

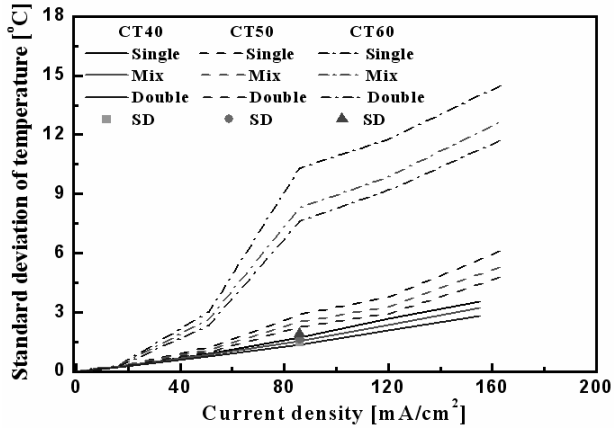

Fig. 9. Standard deviation for the various channel flows.

The water content in the MEA was in the order of mixed > double > single channel. For mixed channel flow at a cell temperature of 40°C, flooding might occur due to the high water content in the MEA. For a cell temperature of 60°C, drying-out might occur due to the poor water production and the vaporization by the hot cell temperature in the MEA. If the gas in the cathode channel moved at lower velocity, the water content would increase due to the increased residence time of the reactants in the gas diffusion layer.

Fig. 7 shows the water activity in the MEA as a function of the current density and cell temperature. When the local activity of water exceeded 1.0, water vapor condensed to form liquid water until the local activity equaled 1.0. When the liquid water was present, and the local activity of water dropped below 1.0, the liquid water evaporated until the local activity equaled 1.0 [28, 29]. When the vapor water condensed in the periphery of the electrode surface, the amount of water film increased with flooding.

Water activity increased with increasing current density for all cell temperature conditions.

The water activity in the MEA was in the highest order of the mixed > double > single channel. The water activity in the MEA at high cell temperature showed little difference with the type of channel flow. However, at low cell temperature, the effect of flow pattern became non-negligible, especially at a cell temperature of 40°C. At this temperature, the water activity of the mixed channel was 0.1 higher than that of the single channel, resulting in increased water content in the MEA.

3.3 Internal temperature and standard deviation for various channel flows

Fig. 8 shows the mean temperature values on the membrane at the cathode as a function of flow pattern and current density. At low current density, the mean temperature values on the membrane were almost the same, regardless of cell temperature. The mean temperature increased with increasing current density for all cell temperatures. At a cell temperature 40°C, the mean temperature on the membrane increased up to 44°C. At the cell temperature of 50 and 60°C, the mean temperatures increased up to 56 and 67°C, respectively, for the starvation condition. The mean temperatures on the membrane were about 10% higher than the cell temperatures.

The mean temperature on the membrane was in the order of single > mixed > double channel. The local temperature at the single channel for the starvation condition was particularly 2°C higher than for the standard condition. The performance of the PEMFC, which is sensitive to a 1°C rise in room temperature, was degraded by the decrease of water content and membrane conductivity.

Fig. 9 shows the standard deviation of the local temperature on the membrane as a function of current density and cell temperature. The standard deviation values of temperature were almost identical regardless of cell temperature for the standard conditions. However, they changed largely along with the cell temperature for the starvation conditions.

In the starvation condition of a cell temperature of 40°C, the standard deviation increased linearly with increasing current density. In the starvation condition of a cell temperature of 50°C, the standard deviation also increased linearly, but the values were larger than those of a cell temperature of 40°C. The discrepancies of the standard deviation between the stan-

dard and starvation conditions were relatively smaller than those of a cell temperature of 60°C. The standard deviation at a cell temperature of 60°C changed dramatically with the increasing current density for the starvation condition. The standard deviation at 85.5 mA/cm^2 increased up to 8.3, which is four times higher than that of the standard condition. This large standard deviation indicates the non-uniform distribution of temperature on the membrane.

The standard deviation of the temperature on the temperature was in the order of single > mixed > double channel.

Compared with the standard condition, the increment of the standard deviation of the local temperature is much larger for a cell temperature of 60°C. Especially in the case of the single channel, the highest increment of the standard deviation value of temperature on the membrane may cause large thermal stresses on the membrane. These results can provide useful information in the design of the PEMFC channel flow.

4. Conclusions

The effect of channel flow pattern on the distribution of the internal properties of the counterflow PEMFC for cathode starvation conditions was investigated through numerical studies and experiments. Based on the numerical and experimental analysis, the following conclusions were obtained:

(1) Mixed serpentine flow gives the fastest velocity of gas in the channel, which is useful for exhausting the condensed water in the channel bend to possibly prevent the channel from flooding.

(2) The local temperature and its standard deviation of a single serpentine flow are the highest among those of other channel flows, and such a condition may cause local thermal stress.

(3) The single serpentine flow is the most sensitive to cathode starvation, while the mixed one is the most durable.

Nomenclature

C	:	Molar concentration (mol/m^3)
CON	:	Conductivity (S/m)
E	:	Open circuit voltage (V)
F	:	Faraday constant, 96487 (C/mol)
I	:	Local current density (A/cm^2)
M	:	Molecular weight (kg/mol)
P	:	Pressure (atm)
Q	:	Volume flow rate (m^3/s)
R	:	Gas constant
T	:	Temperature (K)
t	:	Thickness (mm)
V	:	Cell voltage (V)
X	:	Mole fraction

Greek

α	:	Transfer coefficient
η	:	Overpotential (V)
λ	:	Water content
σ	:	Conductivity (S/m)
ρ	:	Density (kg/m^3)
υ	:	Velocity (m/s)

Subscripts

a	:	Anode
c	:	Cathode
dry	:	Dry state
K	:	Anode or cathode
M	:	Membrane
w	:	Water

References

[1] R. O'Hayre, S. W. Cha., W. Colella and B. Prinz, F., *Fundamentals of fuel cell*, WILEY, U.S.A., (2005) 3-21.

[2] F. Barbir, *Theory and practice of fuel cell*, ELSEVIER, U.S.A., (2005) 1-33.

[3] G. Guvelioglu and H. Stenger, Flow rate and humidification effects on a PEM fuel cell performance and operation, *Journal of Power Sources*, 163 (2006) 882-891.

[4] J. Zhang and Y. Tang, PEM fuel cells operated at 0% relative humidity in the temperature range of 23-120℃, *Electrochimica Acta*, 52 (2007) 5095-5101.

[5] J. Jang, W. Yan and H. Li, Humidity of reactant fuel on the cell performance of PEM fuel cell with baffle-blocked flow field designs, *Journal of Power Sources*, 159 (2006) 468-477.

[6] F. Jing, M. Hou and W. Shi, The effect of ambient contamination on PEMFC performance, *Journal of Power Sources*, 166 (2007) 172-176.

[7] D. H. Jeon, S, Greenway and S. Shimpalee, The effect of serpentine flow-field designs on PEM fuel cell performance, *Journal of Hydrogen Energy*, 33 (2008) 1052-1066.

[8] S. Kaytakoglu and L. Akyalcin, Optimization of parametric performance of a PEMFC, *Journal of Hydrogen Energy*, 32 (2007) 4418-4423.

[9] H. Sun, G. Zhang and L. Guo, Effects of humidification temperatures on local current characteristics in a PEM fuel cell, *Journal of Power Sources*, 168 (2007) 400-407.

[10] S. U. Jeong, E. A. Cho and H. Kim, A study on cathode structure and water transport in air-breathing PEM fuel cells, *Journal of Power Source*, 159 (2006) 1089-1094.

[11] P. C. Sui, S. Kumar and N. Djilali, Advanced computational tools for PEM fuel cell design Part2. Detailed experimental validation and parametric study, *Journal of Power Source*, 180 (2008) 423-432.

[12] Q. Yan, H. Toghiani and H. Causey, Steady state and dynamic performance of PEMFCs under various operating conditions and load changes, Journal of Power Source, 161 (2006) 492-502.

[13] Y. Ishikawa, T. Morita and K. Nakata, Behavior of water below the freezing point in PEFCs, *Journal of Power Source*, 163 (2007) 708-712.

[14] S. Qu, W. Li and M. Hou, The effect of air stoichiometry change on the dynamic behavior of a proton exchange membrane fuel cell, *Journal of Power Source*, 185 (2008) 302-310.

[15] Y. Ishikawa, T. Morita and K. Nakata, Behavior of water below the freezing point in PEFCs, *Journal of Power Source*, 163 (2007) 708-712.

[16] D. Strickland, S. Litster and J. Santiago, Current distribution in polymer electrolyte membrane fuel cell with active water management, *Journal of Power Source*, 174 (2007) 272-281.

[17] A. Taniguchi, T. Akita, and K. Yasuda, Analysis of degradation in PEMFC caused by cell reversal during air starvation, *International Journal of Hydrogen Energy*, 33 (2008) 2323-2329.

[18] W. R. Baumgartner, P. Para and S. D. Fraser, Polarization study of a PEMFC with four reference electrodes at hydrogen starvation conditions, *Journal of Power Source*, 182 (2008) 413-421.

[19] Z. Liu, L. Yang and Z. Mao, Behavior of PEMFC in starvation, *Journal of Power Source*, 157 (2006) 166-176.

[20] W. Yan, H. Li and X. Wang, Effects of serpentine flow field with outlet channel contraction on cell performance of proton exchange membrane fuel cells, *Journal of Power Source*, 178 (2008) 174-180.

[21] X. Liu, H. Guo and F. Ye, Flow dynamic characteristics in flow field of proton exchange membrane fuel cells, *International Journal of Hydrogen Energy*, 33 (2008) 1040-1051.

[22] C. Xu and T. S. Zhao, A new flow field design for polymer electrolyte-based fuel cells, *Electrochemistry Communications*, 9 (2007) 497-503.

[23] J. Kuo, T. Yen and C. Chen, Improvement of performance of gas flow channel in PEM fuel cells, Energy *Conversion and Management*, 49 (2008) 2776-2787.

[24] A. Kazim, H. T. Liu and P. Forges, Modelling of performance of PEM fuel cells with conventional and interdigitated flow field, *Journal of Applied Electrochemistry*, 29 (1997) 1409-1416.

[25] X. Wang, Y. Duan and W. Yan, Effects of flow channel geometry on cell performance for PEM fuel cells with parallel and interdigitated flow fields, *Electrochimica Acta*, 53 (2008) 5334-5343.

[26] X. Wang, Y. Duan and W. Yan, Numerical study of cell performance and local transport phenomena in PEM fuel cells with various flow channel area ratios, *Journal of Power Sources*, 172 (2007) 265-277.

[27] S. Shimpalee, W. Lee and J. W. Van Zee, Predicting the transient response of a serpentine flow-field PEMFC, *Journal of Power Source*, 156 (2005) 355-368.

[28] S. Shimpalee and J. W. Van Zee, Numerical studies on rib&channel dimension of flow-field on PEMFC performance, *International Journal of Hydrogen Energy*, 32 (2007) 842-856.

[29] W. Ying, T. H. Yang and W. Y. Lee, Three-dimensional analysis for effect of channel configuration on the performance of a small air-breathing PEMFC, *Journal of Power Source*, 145 (2005) 572-581.

[30] T. E. Springer, T. A. Zawodzinski and S. Gottesfeld, Polymer electrolyte fuel cell model, Journal of the Electrochemical Society, 138 (8) (1991) 2334-2342.

[31] J. S. Yang and G. M. Choi, Prediction of fuel cell performance and water content in the membrane of a proton exchange membrane fuel cell, Transactions of KSAE, 14 (6) (2006) 151-159.

Gyung-Min Choi obtained his BS and MS degrees in Mechanical Engineering from Pusan National University in 1992 and 1994, respectively. He received his Doctor of Engineering degree from Osaka University in 2002. Dr. Choi is currently a professor at the School of Mechanical Engineering in Pusan National University in Busan. His research interests include combustion, compressor dynamics, and hybrid energy system.

Dong-Soo Ko finished his MS degree in Mechanical Engineering in Pusan National University in 2009. Ko is currently a researcher in LG Electronics.